International Journal of Heat and Mass Transfer 51 (2008) 5260–5268

Contents lists available at ScienceDirect

International Journal of Heat and Mass Transfer

journal homepage: www.elsevier.com/locate/ijhmt

Numerical modeling of bed-to-wall heat transfer in a circulating fluidized bed combustor based on cluster energy balance

Nirmal V. Gnanapragasam [a], B.V. Reddy [b,*]

[a] Department of Mechanical Engineering, University of New Brunswick, Fredericton NB, Canada E3B 5A3
[b] Faculty of Engineering and Applied Sciences, University of Ontario Institute of Technology, Oshawa ON, Canada L1H 7K4

ARTICLE INFO

Article history:
Received 21 August 2007
Received in revised form 21 March 2008
Available online 23 July 2008

Keywords:
Cluster heat transfer
Dispersed phase heat transfer
Energy balance
Temperature profile
CFB combustor
Suspension density
Bed-to-wall heat transfer

ABSTRACT

The bed-to-wall heat transfer in a circulating fluidized bed (CFB) combustor depends on the heat transfer contributions from particle clusters, dispersed/gas phase and radiation from both of them. From the available CFB literature, most of the theoretical investigations on cluster and bed-to-wall heat transfer are based on mechanistic models except a few based on mathematical and numerical approaches. In the current work a numerical model proposed to predict the bed-to-wall heat transfer based on thermal energy balance between the cluster/dispersed phase and the riser wall. The effect of cluster properties and the thermal boundary conditions on the cluster heat transfer coefficient are analyzed and discussed. The fully implicit finite volume method is used to solve the governing equations by generating a 2D temperature plot for the cluster and the dispersed phase control volumes. From this 2D temperature profile, space and time averaged heat transfer coefficients (for cluster, dispersed phase and radiation components) are estimated for different operating conditions. The results from the proposed numerical simulation are in general agreement with published experimental data for similar operating conditions. The results and the analysis from the current work give more information on the thermal behavior of the cluster and dispersed phases, which improves the understanding of particle and gas phase heat transfers under different operating conditions in CFB units.

1. Introduction

Circulating fluidized bed (CFB) combustion is one of the most advanced energy technologies available today for power generation using high ash, high sulfur coals, with reduced emissions of sulfur and nitrogen oxides ($SO_2$and NO_x). Other solid materials such as biomass, municipal waste and wood chips can also be used as the primary fuel to produce high pressure and temperature steam for power generation and process utilities.

The heat transfer phenomena inside the CFB combustor riser column mainly occurs between the suspended bed and the water-wall surfaces which are arranged above the secondary air injection level. The bed-to-wall heat transfer is the combination of convection and radiation heat transfer from cluster and dispersed phases. Investigation on these components gives better understanding of the heat transfer mechanism inside the CFB combustor. From the published investigations reported so far, measurements of the heat transfer components experimentally is quite difficult and thus mechanistic and mathematical models are used to estimate the component heat transfer coefficients and are combined in a specific way to obtain the bed-to-wall heat transfer coefficient which can then be compared with the experimental data. In the mechanistic approach, the cluster heat transfer coefficient is estimated using the correlations, deduced from experimental data by the local estimation of cluster properties combined with the mechanism of cluster behavior. The mathematical approach is done by developing a model by building governing equations from the fundamental mechanism and solving the equations using numerical methods with appropriate assumptions and boundary conditions.

The current work focuses on a mathematical model that involves the energy balance between the cluster and the riser wall. The model also uses correlations for the estimation of cluster properties and a brief account on them as reported in CFB literature is provided here. The cluster voidage (porosity) is found to be in the range of 0.6 to 0.8 reported by Soong et al. [1] and Lints and Glicksman [2]. The shape of the cluster has been described by many researchers including Rhodes et al. [3] as slender strands; Lim et al. [4] noted elliptical and ellipsoidal frontal shapes; infrared images of Noymer and Glicksman [5] show rounded clusters traveling near the riser wall. The size of a cluster for a scale-model CFB was measured by Rhodes et al. [3] and Lim et al. [4] as 0.5–2.0 cm and verified by Noymer and Glicksman [5]. The typical descent velocity for the cluster is between 0.5 and 2.0 m/s as reported by Rhodes et al. [3] and Wang et al. [6] and verified by Noymer and Glicksman [5]. Proximity of the cluster to a wall was observed by

* Corresponding author. Tel.: +1 905 721 3111x3661; fax: +1 905 721 3370.
E-mail addresses: Bale.Reddybv@uoit.ca, bv_reddy@hotmail.com (B.V. Reddy).

0017-9310/$ - see front matter © 2008 Published by Elsevier Ltd.
doi:10.1016/j.ijheatmasstransfer.2008.03.010

Nomenclature

c_p	specific heat, J/kg K
c_{sf}	cluster solid fraction
d_p	mean particle size in the bed, μm
e	emissivity
f	fraction of the wall covered by clusters
f_{cw}	cluster to wall radiation view factor
f_{dw}	dispersed phase to wall radiation view factor
g	acceleration due to gravity, m/s^2
h	bed-to-wall heat transfer coefficient, W/m^2 K
h_c	cluster heat transfer coefficient, W/m^2 K
h_d	dispersed (gas) phase convection heat transfer coefficient, W/m^2 K
h_r	radiation heat transfer coefficient, W/m^2 K
k_c	thermal conductivity of the cluster, W/m K
L_c	cluster characteristic travel length, m
n	cross-sectional average solids volume concentration
Pr	Prandtl number
R	thermal radiation source term coefficient
t_c	cluster residence time, s
T	temperature, K
U_c	cluster descent velocity, m/s
U_t	terminal velocity of solid particles in the bed, m/s
Y	fraction of particles in the dispersed phase

Greek symbols

α	thermal diffusivity of the gas, m^2/s
ε	volumetric void fraction or voidage
$\bar{\varepsilon}$	cross-sectional average voidage at the considered location
μ	dynamic viscosity of the gas, Ns/m^2
ρ	density, kg/m^3

Subscripts

b	bed/suspension
c	cluster
d	dispersed
g	gas
p	particle
w	wall

Abbreviations

CFB	circulating fluidized bed
CEBM	cluster energy balance model
CV	control volume
B.C.	boundary condition
I.C.	initial condition

Lints and Glicksman [2] and is as close as 100 μm from the wall. The existing mathematical models on the cluster hydrodynamics that are reported so far include the work of by Tsuji et al. [7] where cluster patterns are predicted by numerical simulation of particle motion under the effects of inter-particle collision. Noymer and Glicksman [5] modeled the motion of clusters near the wall, treating the clusters as permeable bodies. A hydrodynamic model to predict the formation of clusters from particles in dense phase under the influence of inter-particle forces was developed by Park [8]. Moran and Glicksman [9] simulated the gas flow surrounding a single cluster using the mass conservation and Darcy's law for flow in a permeable body to solve for the pressure and velocity fields. There are several other two-fluid models for particle and cluster flow simulation to predict the hydrodynamics of the clusters and particles in CFB riser column without much information on their heat transfer characteristics. The 2D heat transfer model proposed by Xie et al. [10] reports some results based on energy balance approach but for particles and gas as the control volumes instead of the clusters. The cluster based energy balance and specific analysis relating to the cluster mechanism like the influence of cluster properties on the cluster heat transfer characteristics is not investigated in the existing literature. There is very limited information available on the cluster temperature profile under different operating conditions which would help in understanding how the cluster temperature changes with time for these conditions. The effect of changing thermal boundary conditions on the cluster and dispersed phase heat transfers is not reported so far.

Thus the current work proposes the cluster thermal energy balance model to estimate the cluster convection, dispersed phase convection, cluster radiation, dispersed phase radiation and bed-to-wall heat transfer coefficients in a CFB combustor. This will provide better understanding of the fundamental heat transfer process from particles and gases in the CFB riser column under different operating conditions.

2. Heat transfer mechanism

The heat transfer inside the CFB combustor riser column occurs through particles and combustion gases through convection and radiation in two distinct axial regions of core and annulus. The dilute region in the center forms the "core" region where particles mostly travel upwards along with the gases. Some of the particles re-circulate within the riser by falling into the wall region where the particles start descending along the wall forming the "annulus" region. While descending downward the particles form into groups described qualitatively by Basu and Fraser [11]. The newly grouped particles called "clusters" transfer the bulk heat energy from the particles it contains to the wall. The cluster travels through a certain distance, called the cluster characteristic travel length (L_c) at a descending velocity (U_c) after which it breaks due to several factors including increase in mass and the local forces. The clusters keep forming and breaking in a cyclic process that makes them a major contributor to the heat transfer process from the suspended bed. The particles from the disintegrated clusters along with the surrounding gases in the annular region form the "dispersed phase". At any given instant, there is a continuous exchange of particles from the core to the annulus and annulus to the core, resulting in continuous transfer of heat energy to the wall. Thus the bed-to-wall heat transfer is established through clustered phase convection, dispersed phase convection and the combined radiation from these two phases. Details on the phenomena discussed above is explained in hydrodynamics and heat transfer chapters of Grace et al. [12] and previously reviewed by Basu and Nag [13] from a heat transfer view point.

3. Cluster energy balance model (CEBM)

Energy is transferred from the suspended bed of the CFB combustor to the water walls in the form of heat transfer through convection and radiation. Since the particle concentration is more near the wall in the form of clusters, there is momentary heat conduction inside these particle agglomerates due to the difference in the temperature of the cluster and the bulk temperature of the bed. While conducting heat from the bed momentarily the clusters transfer part of the heat it absorbed to the water wall through convection, again due to temperature difference between the cluster and the wall. The thermal energy balance between the bed and the cluster and between the cluster and the wall are put together

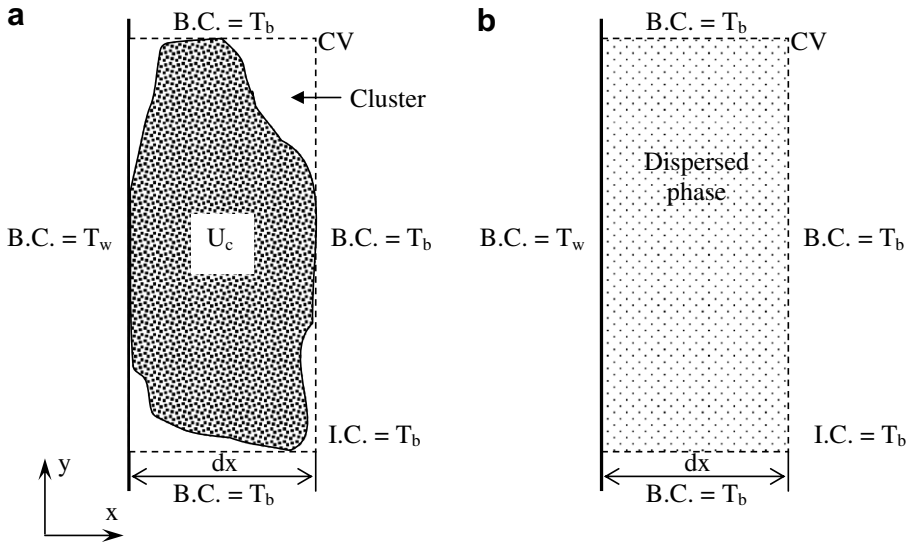

Fig. 1. Control volumes: (a) cluster and (b) equal sized dispersed phase, with boundary conditions of bed and wall temperatures along with the respective initial conditions.

in a single governing equation to estimate the temperature profile of the cluster for a given set of operating conditions. The governing equation for the model is a two-dimensional heat balance equation with a non-linear source term to account for the radiation mode of the cluster heat transfer process. The control volume for the model is shown in Fig. 1. The heat equation for the clustered phase, representing the heat transfer from the cluster to the wall:

$$\underbrace{\rho_c c_{pc}\left(\frac{\partial T_c}{\partial t}\right)}_{\text{rate of change of internal energy}} = \underbrace{\frac{\partial}{\partial x}\left(k_c\frac{\partial T_c}{\partial x}\right)+\frac{\partial}{\partial y}\left(k_c\frac{\partial T_c}{\partial y}\right)}_{\text{net heat increase inside the cluster through conduction}} + \underbrace{R_c T_c^3\frac{\partial T_c}{\partial x}+R_c T_c^3\frac{\partial T_c}{\partial y}}_{\text{net thermal radiation energy generated by the cluster}} \quad (1)$$

The dispersed phase occurs near the walls of the CFB riser due to the continuous breaking and forming of clusters. The particles of a disintegrated cluster and individual particles which do not form clusters along with the combustion gases form the dispersed phase which coexists along with the clusters near to the wall. For the current model the dispersed phase is numerically calculated for the same time span as the cluster phase. That is to find, how much heat is transferred from the dispersed phase for the same time (t_c) as the cluster phase. Applying the energy balance, the governing equation for the dispersed phase becomes.

$$\underbrace{\rho_d c_{pd}\left(\frac{\partial T_d}{\partial t}\right)}_{\text{rate of change of internal energy}} = \underbrace{\frac{\partial}{\partial x}\left(k_d\frac{\partial T_d}{\partial x}\right)+\frac{\partial}{\partial y}\left(k_d\frac{\partial T_d}{\partial y}\right)}_{\text{net heat increase inside the dispersed phase through conduction}} + \underbrace{R_d T_d^3\frac{\partial T_d}{\partial x}+R_d T_d^3\frac{\partial T_d}{\partial y}}_{\text{net thermal radiation energy generated by the dispersed phase}} \quad (2)$$

The behavior of the clusters and dispersed phase in various situations such as other clusters beside the one next to the wall can be handled with appropriate boundary temperature conditions (one such scenario is discussed in Section 8.3).

4. Clustered phase properties

The cluster properties are estimated from the correlations reported in the literature (Basu and Nag [13]). The cross-sectional average voidage of the bed is a function of the bed or suspension density and is given as

$$\bar{\varepsilon} = \frac{\rho_b - \rho_p}{\rho_g - \rho_p} \quad (3)$$

The *cluster solid fraction* (c_{sf}) is the fraction of solid particles residing in the cluster when it is formed and is a function of cross-section bed average voidage ($\bar{\varepsilon}$) from Lints and Glicksman [2]

$$c_{sf} = 1.23(1-\bar{\varepsilon})^{0.54} \quad (4)$$

The cluster solid fraction and the number of clusters formed depend on the suspension density. The *volumetric void fraction or voidage* of the cluster (ε_c) gives the amount of void in the clusters. Two different expressions are used to estimate this voidage the first expression is given by Lints and Glicksman [2];

$$\varepsilon_{c1} = 1 - c_{sf} \quad (5)$$

The second expression for ε_c is from Harris et al. [14] which is a function of average voidage;

$$\varepsilon_{c2} = 1 - \frac{0.58(1-\bar{\varepsilon})^{1.48}}{0.013 + (1-\bar{\varepsilon})^{1.48}} \quad (6)$$

The *characteristic travel length* (L_c), is the distance descended by the cluster before it disintegrates near the wall in a CFB unit and is given by Wu et al. [15];

$$L_c = 0.0178\rho_b^{0.596} \quad (7)$$

The two different *cluster descent velocities* (U_c) are considered. The cluster velocity when the gas flows *around the cluster* as derived by Noymer and Glicksman [16] is

$$U_{c1} = \left(\frac{2}{C_D}\frac{\rho_p}{\rho_g}(1-\varepsilon_c)gd_c\right)^{0.5} \quad (8)$$

The cluster shape used in published mathematical and numerical models are primitive geometries such as sphere and cylinder (Moran and Glicksman [9], Noymer and Glicksman [5,16]). Here the shape is chosen to be a sphere, just to induce a change in the cluster descent velocity and analyze the related influence on the heat transfer characteristics. Thus the expression in Eq. (8) becomes;

$$U_{c2} = \left(\frac{2m_c g}{C_D\rho_g A_c}\right)^{0.5} \quad (9)$$

The mass of the cluster is obtained using the basic definition of mass, $m_c = \rho_c V_c$ where the volume of the cluster is the volume of

a sphere, whose size is varied with values of about 1 to 2 cm being an average size of the cluster reported in Harris et al. [14] for measured values of cluster sizes from different experimental data. The expression in Eq. (9) accounts for the mass and shape of the cluster along with its size. Both the cluster descent velocity expressions given in Eqs. (8) and (9) will be used to get two set of heat transfer values and will be compared and discussed. The *Fractional wall coverage* (f) gives the amount of clusters that will be found near the wall for a given suspension density given by the relation found in Lints and Glicksman [2];

$$f = 3.5(1-\bar{\varepsilon})^{0.37} \tag{10}$$

The cluster control volume and the riser wall can be assumed as two parallel planes such that the cluster radiation view factor becomes,

$$f_{cw} = \frac{1}{\left(\frac{1}{e_w}+\frac{1}{e_c}-1\right)} \tag{11}$$

where the emissivity of the cluster is estimated using the relation given by Grace [17];

$$e_c = 0.5(1+e_p) \tag{12}$$

The cluster radiation source term factor is given as

$$R_c = 4\sigma f_{cw} \tag{13}$$

5. Dispersed phase properties

As mentioned earlier the dispersed phase is the gaseous phase with few dispersed solid particles in it. The estimation of the dispersed phase properties is again based on the cross-section averaged volume void fraction of solid particles and gases involved in the dispersed phase. The thermal conductivity of the dispersed phase is given by

$$k_d = Yk_p + \bar{\varepsilon}k_g \tag{14}$$

The specific heat of the dispersed phase is given by

$$c_{pd} = Yc_{pp} + \bar{\varepsilon}c_{pg} \tag{15}$$

The density of the dispersed phase is given by

$$\rho_d = Y\rho_p + \bar{\varepsilon}\rho_g \tag{16}$$

where $Y = 0.001$ as suggested by Basu [18]. The dispersed phase control volume and the riser wall can be assumed as two parallel planes such that the dispersed phase radiation view factor becomes

$$f_{dw} = \frac{1}{\left(\frac{1}{e_w}+\frac{1}{e_d}-1\right)} \tag{17}$$

where the emissivity of the dispersed phase for isotropic scattering is estimated using the relation given by Brewster [19]

$$e_d = \left[\frac{e_p}{(1-e_p)0.5}\left(\frac{e_p}{(1-e_p)0.5}+2\right)\right]^{0.5} - \frac{e_p}{(1-e_p)0.5} \tag{18}$$

The radiation source term factor for the dispersed phase is given as

$$R_d = 4\sigma f_{dw} \tag{19}$$

6. Assumptions

- Clusters and dispersed phase travel very close to the wall with negligible gap between them and the wall.
- The boundary conditions are constant temperatures, with the bed side boundary at T_b at all times and wall side boundary at T_w at all times. The top and bottom boundary temperatures are changed for specific cases involved in the analysis.
- No collision or influence of other clusters or particles considered.
- Internal heat generation within the control volume is not included, though that can be added as a source term.
- The size and mass of the cluster and dispersed phase remains constant for entire time till t_c.

7. Solving the model

The governing equations (Eqs. (1) and (2)) are solved using the control volume method by using the fully implicit scheme with the above mentioned assumptions. Table 1 gives the physical properties and range of operating conditions used for the model. The control volumes are as shown in Fig. 1. Cluster and dispersed phase control volumes are discretized into 2D finite volume grids with $\Delta x = L/X$ and $\Delta y = L/Y$ where $L = d_c$, $X = Y = 200$ for $d_c = 10d_p$ and $X = Y = 400$ for $d_c = 20d_p$. The calculation starts at $t = 0$ and ends when the time reaches $t = t_c$ where the cluster disintegrates, with a time step of $\Delta t = 0.0005$ and the number of time steps (n) is determined based on t_c, i.e. $n = t_c/\Delta t$. The numerical procedure solves the cluster equation (Eq. (1)) in time and then separately solves the dispersed phase (Eq. (2)) for the *same time*. The solution is obtained using the initial and boundary conditions for both the control volumes (Fig. 1). The resulting solution gives the temperature for all the nodes in the 2D grid from which the heat transfer coefficient is calculated. The discretization of the governing Eqs. (1) and (2) follows the standard procedure of control volume numerical formulation as an integration of Eq. (1) or (2) with time over the cluster or dispersed phase control volume (Fig. 1) gives

$$\begin{aligned}\int_t^{t+\Delta t}\int_{CV}\rho c\frac{\partial T}{\partial t}\mathrm{d}V\,\mathrm{d}t = &\int_t^{t+\Delta t}\int_{CV}\frac{\partial}{\partial x}\left(k\frac{\partial T}{\partial x}\right)\mathrm{d}V\,\mathrm{d}t\\ &+\int_t^{t+\Delta t}\int_{CV}\frac{\partial}{\partial y}\left(k\frac{\partial T}{\partial y}\right)\mathrm{d}V\,\mathrm{d}t\\ &+\int_t^{t+\Delta t}\int_{CV}RT^3\left(\frac{\partial T}{\partial x}\right)\mathrm{d}V\,\mathrm{d}t\\ &+\int_t^{t+\Delta t}\int_{CV}RT^3\left(\frac{\partial T}{\partial y}\right)\mathrm{d}V\,\mathrm{d}t\\ &+\int_t^{t+\Delta t}\int_{CV}s\mathrm{d}V\,\mathrm{d}t\end{aligned} \tag{20}$$

This equation after implementing the finite volume formulation becomes a discretized equation as given here

$$a_P T_P = a_E T_E + a_W T_W + a_N T_N + a_S T_S + a_P^0 T_P^0 + S_C \tag{21}$$

Eq. (21) is solved using the Tri-Diagonal Matrix Algorithm (TDMA) which gives the temperature of every node in the cluster and dispersed phase control volume grids. Based on the number grid

Table 1
Values of physical properties and conditions used in the current model

Solid particle (sand): Incropera and DeWitt [27]	$\rho_p = 2300$ kg/m^3, $k_p = 0.27$ W/mK, $c_{pp} = 800$ J/kgK, $e_p = 0.85$
Gas (air): Flamant [21] $T_{avg}=(T_b+T_w)/2$K	$\rho_g = 351/T_{avg}$ kg/m^3, $k_g = 5.66\times10^{-5}\,T_{avg} + 1.1\times10^{-2}$ W/mK, $c_{pg} = (0.99 + 1.22\times10^{-4}T_{avg})\times10^3$-$(5.68\times10^3 T_{avg}^{-2})\times10^3$J/kgK, $\mu_g = 0.42\times10^{-6}T_{avg}^{2/3}$Ns/m^2
Parameter values:	$d_p = 250$ μm, $U_g = 6$ m/s, $e_w = 0.7$
Operating conditions:	$\rho_b = 5$–40 kg/m^3, $T_b = 1100$ K, $T_w = 600$ K
Initial and boundary conditions:	$T_{init} = T_b, T_{avg}$, $T_{BC} = T_b, T_w, T_{avg}$

points, the solution is grid independent and with multiple sweeps for the TDMA per time step the sensitivity of the numerical solution is nil. The boundary of the control volume facing the wall starts loosing heat to the wall and a temperature profile sets inside the control volume by the time the cluster reaches its disintegration point. From this temperature profile component heat transfer coefficients can be estimated using the conduction-convection relation. The time averaged *cluster* convective heat transfer coefficient is estimated as given below;

$$\overline{h_c} = \mathrm{avg}\left[k_c \frac{(\overline{T_{cx} - T_w})_y}{\Delta x (T_b - T_w)}\right]_t \tag{22}$$

where x in T_x represents the last node of the control volume, next to the riser wall. The temperature difference is along the x-direction (width of the control volume) and then they are averaged along y-direction (height of the control volume). The thermal conductivity of the cluster (k_c) is estimated from the expression given by Gelperin and Einstein [20]. The time averaged *dispersed phase* (gas) convective heat transfer coefficient is estimated similarly as

$$\overline{h_d} = \mathrm{avg}\left[k_d \frac{(\overline{T_{dx} - T_w})_y}{\Delta x (T_b - T_w)}\right]_t \tag{23}$$

The time averaged *radiation* heat transfer coefficient for the cluster is given below

$$\overline{h_{rc}} = \mathrm{avg}[\sigma f_{cw}(T_{cx} + T_w)(T_{cx}^2 + T_w^2)]_t \tag{24}$$

The time averaged *radiation* heat transfer coefficient for the dispersed phase is given below

$$\overline{h_{rd}} = \mathrm{avg}[\sigma f_{dw}(T_{dx} + T_w)(T_{dx}^2 + T_w^2)]_t \tag{25}$$

And the time averaged *total* heat transfer coefficient for bed-to-wall heat transfer is calculated as

$$\bar{h} = f\overline{h_c} + (1-f)\overline{h_d} + f\overline{h_{rc}} + (1-f)\overline{h_{rd}} \tag{26}$$

The heat transfer coefficient is estimated for different set of operating conditions and cluster properties for analysis and discussion.

8. Results and discussion

The cluster and bed-to-wall heat transfer coefficients are estimated for a range of suspension densities (5–40 kg/m^3) and for different cluster properties and operating conditions. The thermo-physical properties of the solid particles are as follows ρ_p = 2300 kg/m^3, k_p = 0.27 W/m K, c_{pp} = 800 J/kg K and e_p = 0.85. The thermo-physical properties of the gas are calculated using correlations from Flamant [21]. The bed and wall temperatures are at 1100 K and 600 K respectively. The particle size d_p = 250 μm and the superficial gas velocity of 6 m/s. The results are discussed for parameters that mainly affect the cluster heat transfer coefficient.

8.1. Effect of operating conditions

The cluster properties and the local bed conditions are functions of suspension density, thus making it the primary operating condition for the heat transfer model in the CFB combustor. For the current analysis all the model parameters and cluster properties are plotted with respect to the suspension density. The temperature profile of the cluster at time t_c is shown in Figs. 2 and 3 with the indication of bed and wall sides of the cluster. The profile in Fig. 2 gives the average of temperatures of all the vertical nodes (i.e., averaged along the height) into a row of temperature across the width of the cluster which is plotted for three different suspension densities. The temperature profile gives a better picture of the heat transfer process from one side to the other side of the cluster

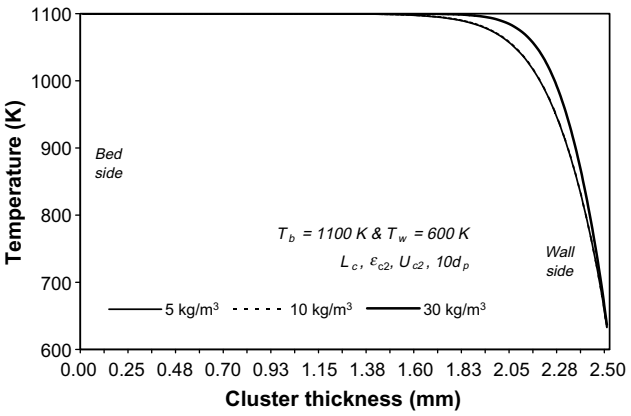

Fig. 2. Cluster temperature profile at t_c averaged along the height of the cluster for a $10d_p$ cluster size at three different *suspension densities*.

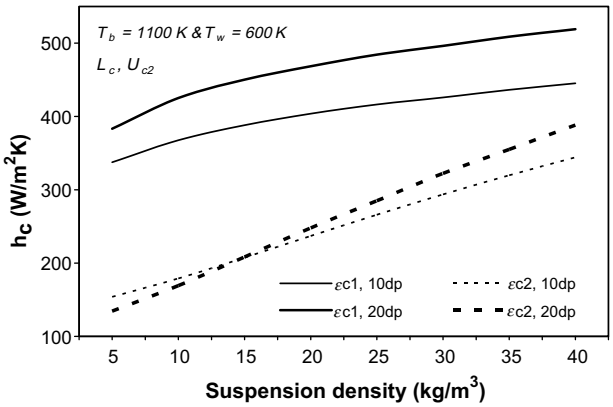

Fig. 3. Cluster heat transfer coefficient variation with change in *cluster voidage* estimated based on the expressions of Lints and Glicksman [2] (ε_{c1}) and Harris et al. [14] (ε_{c2}).

making it easier to discuss the cluster heat transfer coefficient. The cluster heat transfer coefficient increases with increase in suspension density as shown in Fig. 3 for the given conditions. This is due to the presence of more particles in the cluster which are formed at a higher suspension density. The presence of more particles inside the cluster increases its bulk temperature through conduction within the cluster. This can be observed through the temperature profile across the thickness of the cluster (near the wall side) as shown in Fig. 2 for three different suspension densities. The 30 kg/m^3 curve has higher temperature due to higher particle concentration. It also shows that the cluster formed at lower suspension density has higher gradient in temperature thus limiting heat transfer to the wall. The temperature gradient near the 'wall side' is used in calculating the cluster heat transfer coefficient as given in Eq. (20). Apart from the suspension density the other operating condition that affects the heat transfer coefficient is the bed temperature and the details are reported previously (Vijay and Reddy [22], Basu and Nag [13], Wu et al. [15]).

8.2. Effect of cluster parameters

(i) <u>*Cluster Voidage*</u>: The cluster voidage specifies the amount of gas present inside the cluster, estimated using the correlations of Lints and Glicksman [2] in Eq. (5) (ε_{c1}) and Harris et al. [14] in Eq. (6) (ε_{c2}) are functions of the suspension density, and thus have a distribution with increase in suspen-

sion density. For the given suspension density distribution (5 to 40 kg/m^3) the cluster voidage values of ε_{c1} ranges from 0.957 to 0.863 and values of ε_{c2} ranges from 0.996 to 0.908. The cluster with ε_{c1} has lower voidage or higher particle concentration and thus higher cluster heat transfer coefficient as shown in Fig. 3. The cluster with ε_{c2} has more voidage and thus has lower cluster heat transfer coefficient. Within the ε_{c1} voidage distribution, the heat transfer coefficient varies significantly for changes in cluster size because of higher solid concentration inside the cluster. The cluster size does not affect the heat transfer values of cluster with ε_{c2} because of higher voidage in the cluster for lower suspension density. The cluster with ε_{c2} shows better sensitivity in heat transfer values with change in suspension density than the cluster with ε_{c1}. This is due to lower voidage in the cluster with ε_{c1}, that it has higher temperature even at low suspension density (in Fig. 2 the 5 kg/m^3 curve for ε_{c1}). The cluster temperature profile for the two cluster voidage (ε_{c1} and ε_{c2}) at a particular suspension density is shown in Fig. 4 for two different cluster sizes (10d$_p$ and 20d$_p$). The cluster with ε_{c1} has low temperature gradient for both cluster sizes due to higher particle concentration based on its voidage distribution and thus will have higher heat transfer coefficient (Fig. 3). The cluster with ε_{c2} has more temperature gradient along the thickness of the cluster and thus has lower heat transfer coefficient. These two cluster voidage distributions shows that even a small change in cluster voidage influences the cluster heat transfer coefficient significantly thus making it an important parameter in modeling cluster heat transfer estimation. The proper estimation of this voidage is essential for realistic cluster heat transfer coefficient prediction.

(ii) *Cluster size*: The cluster size is often neglected in cluster heat transfer analysis which in fact gives more information regarding the relationship between cluster properties and the impact on its heat transfer characteristics. The cluster size is included in the model at two places. One in the cluster descent velocity estimation for calculating the cluster Reynolds number and the other place is the size of the 2D grid which equals the diameter of the cluster. For comparison of heat transfer values among different cluster sizes for the current model four cluster dimensions are used. They are 10 and 20 times the size of the solid particle (d_p = 250 μm) having two different clusters of 2.5 mm and 5 mm in diameter, which is within the range of measured values of cluster sizes occurring in experimental CFB units as reported in Harris et al. [14]. The variations in cluster heat transfer coefficients for these two clusters are shown in Fig. 3. The larger cluster (20d$_p$) has higher cluster heat transfer coefficients than the smaller cluster (10d$_p$) for both cluster voidage. This is because for a given suspension density, the solids concentration in a larger cluster will be higher than a smaller cluster. The large cluster with ε_{c1} in Fig. 3 indicates a cluster with higher solids concentration. For cluster with ε_{c2} there is very little difference in heat transfer values for the two cluster sizes. The temperature profile in Fig. 4 also supports the higher heat transfer to the wall from larger clusters due to large difference in temperatures between the cluster wall and the riser wall.

(iii) *Cluster descent velocity*: The cluster descent velocity is an important characteristic of the cluster since its value affects the resident time of the cluster near the wall and thus the heat transfer coefficient. The cluster descent velocity in the current model is estimated using two different expressions as given in Eqs. (8) and (9). The value of descent velocities estimated from these two equations with respect to the suspension density range (5–40 kg/m^3) has the following range: U_{c1}: 1.2–5.6 m/s and U_{c2}: 0.4–1.6 m/s. From the values, it is evident that the cluster with U_{c1} descends almost twice as fast as the cluster with U_{c2}. The value of cluster resident time (t_c) for the respective velocities shows that the faster the cluster descends the less time it stays near the wall. From the t_c values for U_{c1} and U_{c2} it is observed that, the U_{c2} cluster will stay twice as long as the U_{c1} cluster near the wall. This will induce a larger temperature gradient inside the cluster descending at U_{c2} resulting in lower cluster heat transfer coefficient values. This can be observed in the cluster heat transfer values for the two velocity distributions shown in Fig. 5. The dense cluster (ε_{c1}) with U_{c1} has higher heat transfer values due to smaller gradients in temperature and the fact that at higher suspension densities this cluster will have more particles than ε_{c2} cluster (which has higher voidage for the same suspension density). The fact that the U_{c1} cluster has higher heat transfer than the slower U_{c2} cluster in Fig. 5 shows that the rate of heat transfer is higher and the cluster has very little time to cool before it breaks. The heat transfer value for the slower cluster (U_{c2}) is lower may be due to loss of heat since it stays near the wall for longer time.

(iv) *Cluster characteristic descent length*: The cluster descent length as given in Eq. (7) as a function of suspension density underpredicts the length and to have better prediction for larger CFB units, a length 10 times L_c in Eq. (7) is suggested as reported in Wu et al. [15] and Basu and Nag [13]. This is done mainly to account for the discrepancy when cluster descends longer than normal distances especially in commercial CFB

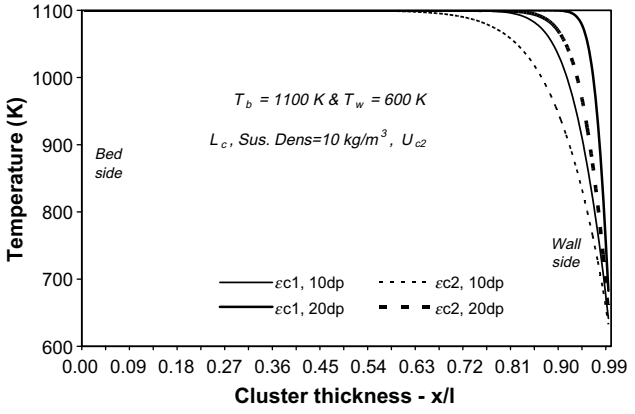

Fig. 4. Cluster temperature profile at t_c averaged along the height of the cluster for the two different *voidage* (ε_{c1} and ε_{c2}) and *cluster sizes* (10d$_p$ and 20d$_p$).

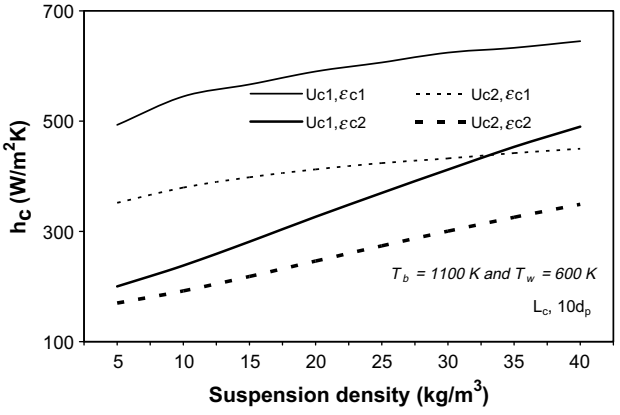

Fig. 5. Cluster heat transfer coefficient variation with suspension density for two different*cluster descent velocities* estimated based on the expressions of Noymer and Glicksman [16] (U_{c1}) and the modified form (U_{c2}) along with two different *clusters voidage* (ε_{c1} and ε_{c2}).

combustors. With increasing cluster descent length the cluster heat transfer coefficient decreases suggesting that the cluster cools down as it travels longer. If the cluster descends or stays as a cluster far enough, it cools down as shown in Fig. 6 where the change in cluster heat transfer coefficient with time is given for two different cluster descent lengths (T_b, L_c and T_b, 10 L_c curves). The cluster for L_c distance looses heat to the wall rapidly from $t = 0$ till $t = t_c$ thus showing better heat transfer to the wall. Whereas the cluster for $10L_c$ distance, has almost the same heat transfer coefficient from the start till the end, which shows that, the cluster that has traveled 10 times longer than another cluster with same properties, has very little change in heat transfer with time after certain distance.

8.3. Effect of initial and boundary temperatures of the control volume

The cluster as it forms has an initial temperature which is the accumulated bulk temperature of all the solid particles inside the cluster. This temperature influences the temperature profile of the cluster as it descends till it breaks. There are chances where a cluster might be formed with some particles having transferred its heat energy already to the wall when they form part of the cluster. Thus the average initial temperature of the cluster may not be the same as bed temperature always. The other reason will be the cluster being near the wall, which has considerably low temperature than the bed side of the cluster. If a cluster has an average of bed and wall temperature as its initial temperature (i.e. $T_{avg} = 850$ K) the change in cluster heat transfer coefficient with time is shown in Fig. 6 for two different cluster descent lengths (T_{avg}, L_c and T_{avg}, $10L_c$ curves). The cluster which travels for L_c distance starts cooling from the start and begins to increase its heat transfer near the end (near t_c). Whereas the cluster which travels for 10 times longer distance ($10L_c$) starts to gain heat from the beginning due to the boundary condition (top, bottom and right in Fig. 1) which is at bed temperature. Thus the cluster which forms with particles having average temperature will have lower heat transfer coefficient and starts gaining heat if it travels for longer distance.

Apart from the initial temperature of the cluster, its top and bottom boundary temperatures (shown in Fig. 1) also affect its heat transfer characteristics. Fig. 7 shows the change in cluster heat transfer coefficient with suspension density for four different cluster temperature conditions as given below: Here T_b is bed temperature and T_{avg} is average of bed and wall temperatures. Left side boundary is always T_w and right side boundary is always T_b (Fig. 1).

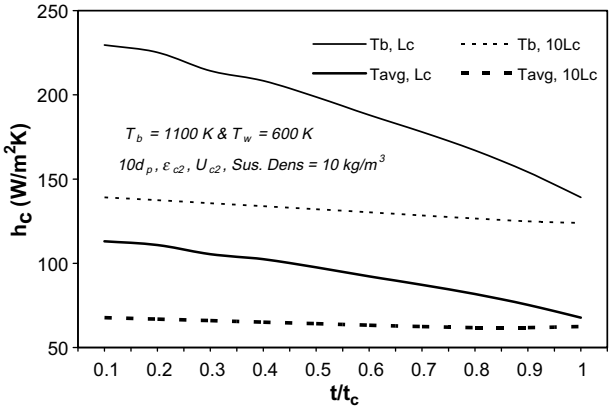

Fig. 6. Change in the cluster heat transfer coefficient with *time* compared here for two different *cluster initial temperatures* (T_b and T_{avg}) and *cluster descent lengths* (L_c and $10L_c$).

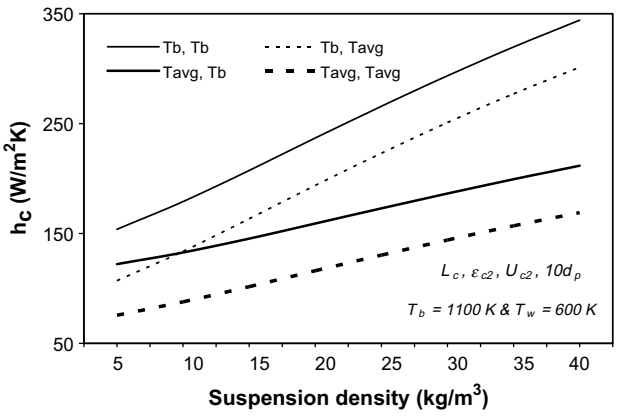

Fig. 7. Change in the cluster heat transfer coefficient with suspension density compared for two different *cluster initial temperatures* (T_b and T_{avg}) and *cluster top and bottom boundary temperatures* (T_b and T_{avg}).

(i) T_b,T_b: The cluster has both initial and top and bottom boundary conditions equal to T_b. This situation occurs when there are mostly clusters or dense clouds of particles near and around the cluster under discussion. So the cluster only looses heat to the wall. So it has higher heat transfer coefficient as shown in Fig. 7. Also from Fig. 8 the temperature profile for this condition shows no change except near the wall.

(ii) T_b,T_{avg}: The cluster has T_b as the initial temperature and T_{avg} as top and bottom boundary condition. Here the cluster has T_b when it forms and descends in a region with dispersed phase or gas such that the top and bottom boundary temperature becomes T_{avg}. Here the cluster looses heat to the wall as well on top and bottom. So it has lower heat transfer coefficient (Fig. 7) with respect to the previous condition. The vertical averaged temperature profile for this condition is shown in Fig. 8, where the cluster has an average of 1000 K except near the wall due to the higher temperature difference between the wall and the cluster.

(iii) T_{avg},T_b: The cluster has T_{avg} as the initial temperature and T_b as top and bottom boundary condition. The cluster forms with particles already cooled and the initial temperature is T_{avg} but is surrounded by hot environment (other clusters, dense particle clouds, closer to the bed, etc). The cluster will loose heat to the wall and will gain heat from the top, bottom and left boundaries. It acts as a good heat exchanger with the temperature profile as shown in Fig. 8, where it has higher temperature level compared to the previous case due to the

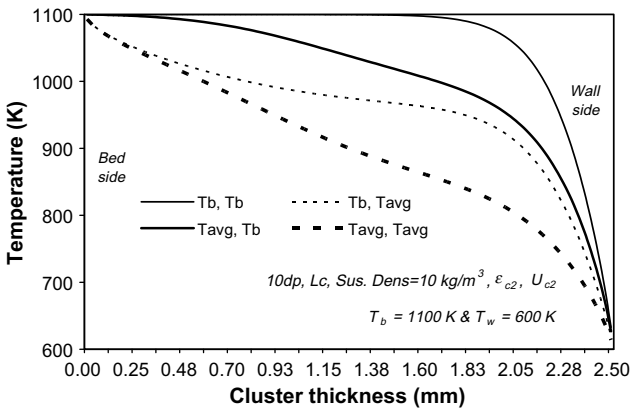

Fig. 8. Vertical averaged cluster temperature profile at t_c for changes in *cluster initial temperatures* (T_b and T_{avg}) and *cluster top and bottom boundary temperatures* (T_b and T_{avg}).

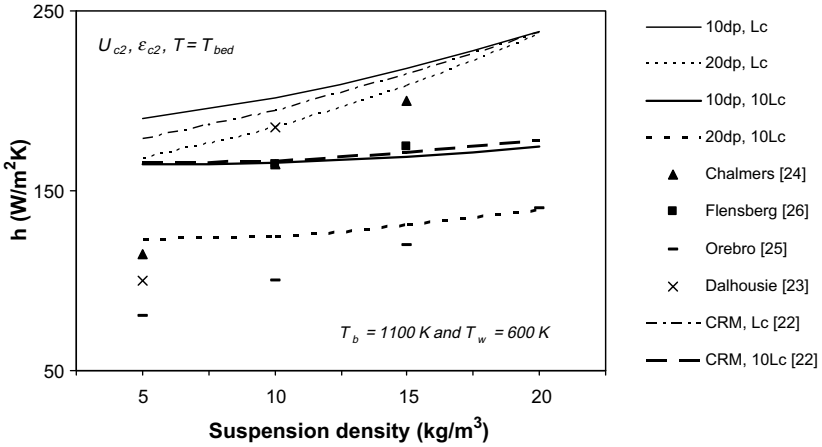

Fig. 9. The bed-to-wall heat transfer coefficient compared with *experimental data* and *CRM of Vijay and Reddy [22]* for two different *cluster descent lengths* (L_c and 10 L_c) and *cluster sizes* ($10d_p$ and $20d_p$) with *bed temperature* (T_{bed}) as the initial and boundary temperature for the cluster.

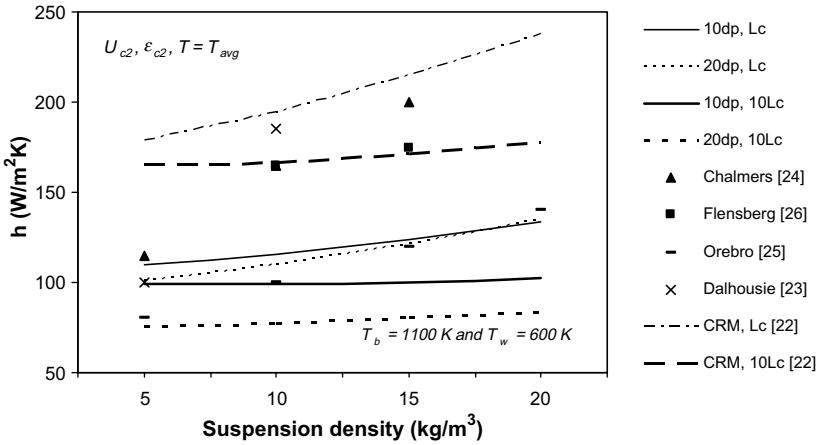

Fig. 10. The bed-to-wall heat transfer coefficient compared with *experimental data* and *CRM of Vijay and Reddy [22]* for two different *cluster descent lengths* (L_c and $10L_c$) and *cluster sizes* ($10d_p$ and $20d_p$) with *average of bed and wall temperatures* (T_{avg}) as the initial and boundary temperature for the cluster.

influence of top and bottom boundary temperatures. The cluster heat transfer coefficient for this cluster is lower (Fig. 7) than the previous two cases, since for the cluster to gain as much heat or become equal in temperature like the previous clusters, it will take more time than t_c.

(iv) T_{avg}, T_{avg}: The cluster has T_{avg} as the initial temperature and T_{avg} as top and bottom boundary condition. The cluster has very low potential for heat transfer in this case since it has lower temperature to start with and is surrounded by low temperature medium (gas, dispersed phase, broken cluster particles, etc). It continuously looses heat to the wall and very little heat gain from the top and bottom boundaries. So the heat transfer coefficient is the lowest (Fig. 7) for this case and the cluster has low average temperature across its thickness as shown in Fig. 8 due to the low initial and boundary temperatures.

Thus the influence of cluster initial and boundary temperatures on the cluster heat transfer coefficient is evident from the cases discussed. In commercial CFB combustors, majority of the clusters which form may not 'see' the bed, i.e. may not have the same temperature as the bulk bed while it is forming, but a lower value due to the randomly changing radial temperature profile across the combustor especially in the annulus and core interface region. The boundary temperature analysis becomes an important way to check the influence of the presence of the bulk temperatures of other clusters, particles and gas surrounding the cluster.

8.4. Effect of the energy balance on bed-to-wall heat transfer coefficient (h)

The bed-to-wall heat transfer coefficient is estimated as given in Eq. (24) by including the cluster and dispersed phase heat transfer coefficients with the respective radiation components. Fig. 9 shows the change in bed-to-wall heat transfer coefficient with suspension density for two different cluster sizes ($10d_p$ and $20d_p$) and cluster descent lengths (L_c and $10L_c$) with T_b as the initial and boundary temperatures, is compared with experimental data along with the results from the cluster renewal mechanistic model (CRM with $10d_p$ clusters from Vijay and Reddy [22]). The larger clusters have lower heat transfer coefficients for the same cluster descent lengths with the current model predicting higher than the experimental as well as CRM values. On the other hand Fig. 10 shows different trends in the bed-to-wall heat transfer values for the same set with T_{avg} as the initial and boundary temperatures of the cluster (CRM values remain the same). The clusters descending longer (i.e. for $10L_c$ distance) does not change with increase in suspension density and are in good proximity with the experimental data especially for the larger cluster. This suggests that in commercial CFB units the clusters must be large clusters

(in the order of $20d_p$ or more) with average initial temperatures and descending longer ($10L_c$) than the predicted value.

9. Conclusion

In the current work a numerical model based on cluster and dispersed phase energy balance is proposed to estimate cluster and bed-to-wall heat transfer coefficients for different cluster properties and bed operating conditions. Based on the comparison of the model results with the experimental data the following conclusions are drawn:

- The cluster parameters such as cluster voidage, descent velocity, descent length and size have significant influence on cluster and bed-to-wall heat transfer phenomena.
- The difference in the heat transfer values based on the two different cluster voidage and cluster velocity correlations suggests the need for better prediction of cluster properties, for proper estimation of cluster and bed-to-wall heat transfer coefficients.
- The cluster initial and boundary temperatures influences the cluster and bed-to-wall heat transfer coefficients and provides evidence that a cluster may not have the same temperature as the bed when it starts forming due to the presence of other clusters, particles and gas.
- The comparison with cluster renewal mechanistic model shows the improvement achieved in the current model towards bed-to-wall heat transfer estimation.
- The trends from the present model predictions are in reasonable agreement with the published experimental data for the same range of operating conditions.

Acknowledgements

The authors kindly acknowledge the financial support for the present project from Natural Sciences and Engineering Research Council of Canada through the Discovery Grant Program. The work was done at Department of Mechanical Engineering, The University of New Brunswick, Fredericton, New Brunswick, Canada.

References

[1] C.H. Soong, K. Tuzla, J.C. Chen, Identification of particle clusters in circulating fluidized beds, in: A.A. Avidan (Ed.), Circulat. Fluidized Bed Technol., vol. IV, Engineering Foundation, NY, 1993, pp. 615–620.
[2] M.C. Lints, L.R. Glicksman, Parameters governing particle to wall heat transfer in a circulating fluidized bed, in: A.A. Avidan, (Ed.), Circulating Fluidized Bed Technology, vol. IV, AIChE, NY, 1994, pp. 63–82.
[3] M. Rhodes, H. Mineo, T. Hirama, Particle motion at the wall of a circulating fluidized bed, Powder Technol. 70 (1992) 207–214.
[4] K.S. Lim, J. Zhou, C. Finley, J.R. Grace, C.J. Lim, C.M.H. Brereton, Cluster descending velocity at the wall of circulating fluidized bed risers, in: M. Kwauk, J. Li (Eds.), Circulating Fluidized Bed Technology, vol. V, Chemical Industry Press, Beijing, 1996, pp. 218–223.
[5] P.D. Noymer, L.R. Glicksman, Cluster motion and particle-convective heat transfer at the wall of a circulating fluidized bed, Int. J. Heat Mass Transfer 41 (1998) 147–158.
[6] T. Wang, Z.J. Lin, C.M. Zhu, D.C. Liu, S.C. Saxena, Particle velocity measurements in a circulating fluidized bed, AIChE J. 39 (1993) 1406–1410.
[7] Y. Tsuji, T. Tanak, S. Yonemura, Cluster patterns in circulating fluidized beds predicted by numerical simulation (discrete particle model versus two-fluid model), Powder Technol. 95 (1998) 254–264.
[8] J.Y. Park, The clustered dense phase model for group A fluidization: I. Dense phase hydrodynamics, Chem. Eng. Sci. 58 (2003) 193–202.
[9] J.C. Moran, L.R. Glicksman, Experimental and numerical studies on the gas flow surrounding a single cluster applied to a circulating fluidized bed, Chem. Eng. Sci. 58 (2003) 1879–1886.
[10] D. Xie, B.D. Brown, J.R. Grace, C.J. Lim, Two-dimensional model of heat transfer in circulating fluidized beds. Part I: Model development and validation, Int. J. Heat Mass Transfer 46 (2003) 2179–2191.
[11] P. Basu, S. Fraser, Circulating Fluidized Bed Boiler – Design and Operation, Butterworth-Heinemann Publishers, Stoneham, 1991. pp. 31–33.
[12] J.R. Grace, A.A. Avidan, T.M. Knowlton (Eds.), Circulating Fluidized Beds, Blackie Academic and Professional, London, 1997, pp. 261–307.
[13] P. Basu, P.K. Nag, Heat transfer to walls of a circulating fluidized bed furnace, Chem. Eng. Sci. 51 (1996) 1–26.
[14] A.T. Harris, J.F. Davidson, R.B. Thorpe, The prediction of cluster properties in the near wall region of a vertical riser (200157), Powder Technol. 127 (2002) 128–143.
[15] R.L. Wu, J.R. Grace, C.J. Lim, A model for heat transfer in circulating fluidized beds, Chem. Eng. Sci. 45 (1990) 3389–3398.
[16] P.D. Noymer, L.R. Glicksman, Descent velocities of particle clusters at the wall of a circulating fluidized bed, Chem. Eng. Sci. 55 (2000) 5283–5289.
[17] J.R. Grace, Fluidized bed heat transfer, in: G. Hestroni (Ed.), Handbook of Multiphase Flow, McGraw-Hill, Hemisphere, Washington, DC, 1982, pp. 9–70.
[18] P. Basu, Heat transfer in fast fluidized bed combustors, Chem. Eng. Sci. 45 (1990) 3123–3136.
[19] M.Q. Brewster, Effective absorptivity and emissivity of particulate sender with application to a fluidized bed, Trans. ASME 108 (1986) 710–713.
[20] N.I. Gelperin, V.G. Einstein, Heat transfer in fluidized beds, in: J.F. Davidson, D. Harrison (Eds.), Fluidization, Academic Press, London, 1971, pp. 471–540.
[21] G. Flamant, Tranfert de chaleur couples dans les lits fluidises a haut temperature, Application a la conversion thermique de l'energie solaire, these de docteur Ea-Science 93 (1985).
[22] G.N. Vijay, B.V. Reddy, Effect of dilute and dense phase operating conditions on bed-to-wall heat transfer mechanism in a circulating fluidized bed combustor, Int. J. Heat Mass Transfer 48 (2005) 3276–3283.
[27] F.P. Incropera, D.P. Witt, Fundamentals of Heat and Mass Transfer, John Wiley and Sons, 2002.